Journal of Archaeological Science 67 (2016) 7–13

Contents lists available at ScienceDirect

Journal of Archaeological Science

journal homepage: http://www.elsevier.com/locate/jas

Friendly fire: Engineering a fort wall in the Iron Age

Fabian B. Wadsworth [a, *], Michael J. Heap [b], Donald B. Dingwell [a]

[a] Earth and Environmental Sciences, Ludwig-Maximilians-Universität, Theresienstr. 41, 80333 Munich, Germany
[b] Géophysique Expérimentale, Institut de Physique de Globe de Strasbourg (UMR 7516 CNRS, Université de Strasbourg/EOST), 5 rue René Descartes, 67084 Strasbourg cedex, France

ARTICLE INFO

Article history:
Received 26 August 2015
Received in revised form
15 January 2016
Accepted 23 January 2016
Available online 13 February 2016

Keywords:
Cristobalite
Uniaxial compressive strength
Iron Age technology
Darley Dale sandstone

ABSTRACT

There is widespread evidence that the walls of Iron Age forts across Europe were set on fire, causing partial melting of the stonework followed by either recrystallization or glass formation on cooling – a process termed "vitrification". The motivation for fort wall firing has remained speculative since its first description in 1777. Since the suggestion of MacKie (1969) that fort vitrification might destabilize fort walls, the debate as to motives has focused on combative or destructive intentions. Here, a multidisciplinary analysis of experimental fort wall samples shows that in fact vitrification results in strengthening, not weakening. The strengthening involves diffusive and viscous sintering of material aggregates and size-dependent heat transfer. These new results support a long-since-dismissed idea that Iron Age fort walls were intentionally set ablaze in order to fortify the walls.

1. Introduction

Archaeological science strives to constrain the practices and motives of people in antiquity. One exquisitely preserved example of their doings is represented by the so-called "vitrified" Iron Age forts of Western Europe. Vitrified is a term is used to describe a fort wall construction that contains glass or a devitrified product thereof and usually interpreted to be the result of high temperature activity. While hundreds of examples of vitrified Iron Age forts exist across Europe, the motive for their firing and resultant vitrification remains an outstanding question in archaeology. Of late there is general consensus that fort wall vitrification was intentional (Christison, 1898; Nisbet, 1974; Youngblood et al., 1978). Four categories of intentional motive have been proposed (Wadsworth et al., 2015); (a) strengthening of the stonework (Brothwell et al., 1974; Christison, 1898; Nisbet, 1974), (b) hostile attack with destructive intent (Aylwin Cotton, 1954; Small and Cottam, 1972), (c) post-occupancy destruction by the builders of the wall (MacKie, 1969; Ralston, 1986), or (d) ritual or cultural practices with other motives (Bowden, and McOmish, 1987).

That vitrification was an intentional process for strengthening the fort walls (here: "the engineering argument") has been considered "untenable" since Mackie (1969, 1976), citing the large-scale experimental vitrification of a stone wall by Childe and Thorneycroft (1938), proposed that burning of a wall will cause local instability and collapse. This has led to a paradigm guiding subsequent work toward a combative (Aylwin Cotton, 1954; MacKie, 1976; Nisbet, 1974) or destructional (MacKie, 1969; Ralston, 2007) intent for vitrification. That, in turn has been supported by evidence that vitrification occurred toward the end of occupation (Gifford, 1992; Kresten and Goedicke, 1996; MacKie, 1976) rather than during construction.

Ample evidence exists to demonstrate that exposure to high temperature generally decreases the bulk strength of building materials by inducing microcracks (Hajpál, 2002; Heap et al., 2012). Vitrification however, achieved by the significant sintering of blocks and interstitial particles in dry-stone fort walls in the presence of a partial melt, is another matter. Based on evidence from sintering experiments on glass fragments we have previously shown that such sintering results in a dramatic *increase* in material strength (Vasseur et al., 2013). We therefore speculate that the firing of Iron Age fort walls to temperatures where significant vitrification is achieved through sintering is likely to result in significant strengthening.

Here we provide experimental evidence that firing of Iron age forts may have led to their strengthening after all. The new evidence is based on controlled experiments on heat-treated samples of a sandstone and a powder thereof – designed to represent, respectively, the blocks and the disaggregated mortar that comprise a typical Iron Age fort wall.

* Corresponding author.
E-mail address: Fabian.wadsworth@min.uni-muenchen.de (F.B. Wadsworth).

http://dx.doi.org/10.1016/j.jas.2016.01.011

2. Materials and methods

Darley Dale sandstone (Derbyshire, England) was chosen for this study due to its widespread use and characterization in the rock deformation literature and its textural and compositional homogeneity (Brantut et al., 2014). It also derives from the same stratigraphic stage in the Carboniferous period as the Parkgate sandstone from which the Wincobank Iron Age vitrified fort was constructed (Wadsworth et al., 2015). The initial mineral assemblage of Darley Dale sandstone comprises quartz (69 wt.%), feldspar (26 wt.%), clay (2 wt.%) and mica (2 wt.%) (Heap et al., 2009; Wu et al., 2000) and the diameter of the particles (or grains) in the sandstone blocks varies between ~80 and 800 μm (Wu et al., 2000).

Differential scanning calorimetry (DSC) in combination with thermogravimetric analysis was performed using a Netzsch Pegasus 440C simultaneous thermal analyzer (STA). These techniques show the evolution of the specific heat capacity and the sample mass during high temperature treatment, which are critical for the interpretation of macroscopic property evolution such as material strength. Samples of Darley Dale sandstone were slowly crushed by hand in an agate mortar to avoid the heat produced during mechanical milling techniques and then sub-samples of 40–55 mg were placed in lidded platinum crucibles and heated at 10 or 25 °C min^{-1} to 1400 °C. Two identical cooling and heating cycles were performed for each experiment to identify any potential changes in sample state after initial heating. An empty-crucible baseline was subtracted and the specific heat capacity was obtained by the standard ratio technique by comparison with identical runs with a pure sapphire standard of near-identical mass. We note that the sample mass used is necessarily small to ensure precision and repeatability of the results and repeat runs were performed to confirm representativeness of the bulk sample behaviour.

Optical dilatometry was performed in a Hesse Instruments® heating stage in order to assess sample volume changes during heating. Samples of sieved, <63 μm, hand-crushed sandstone particles were formed into cylindrical free-standing samples (Wadsworth et al., 2014) and were heated at 10 or 25 °C min^{-1} to 1400 °C; conditions identical to the thermal analysis described above. Images of the sample were captured parallel to the cylinder's axis of rotation. Continuous measurements of pixel area, height and width (continuous data) of the sample were obtained at 1 Hz, while images were taken every ~10 °C (discrete data). The continuous data were converted to volume by using a cylindrical assumption while the discrete data were processed by the solid-of-rotation method. The solid-of-rotation involves the numerical integration of the sample radius R (detected from binary images using a Canny edge detection algorithm) around a central axis of symmetry in the y-direction over the sample height L such that the volume $V = \int_0^L \pi R^2 dy$. The volumes in voxels from both methods were converted to porosity ϕ by knowing an initial porosity ϕ_i. The initial porosity was determined by the volume, mass and powder-density where the powder-density was measured in a helium pycnometer. Then $\phi = 1 - V_i(1 - \phi_i)/V$ where V_i is the initial sample volume.

Cylindrical cores of Darley Dale sandstone were drilled from a single block to 20 mm diameter and precision ground to a nominal length of 40 mm. These were heated at 10 °C min^{-1} in a box furnace to target temperatures 800–1400 °C and then held isothermally for either 10 min or 5 h before cooling to room temperature at a rate limited by the furnace. Hand-crushed powder of the same sandstone was loosely packed into alumina ceramic tubes. The alumina tubes were 60 mm height with an internal diameter of 40 mm and an external diameter of 44 mm. These tubes were carefully placed in the box furnace and heated to the same target temperatures for an isothermal hold period of 5 h, before being cooled and then drilled and ground to dimensions identical to the cylindrical cores of sandstone described above. Helium pycnometric determination of connected sample porosity was conducted on samples prior to and following heat treatment. Finally, the uniaxial compressive strength, a standard metric for material strength, of intact (i.e. untreated) Darley Dale sandstone and of all thermally treated cores was determined using a uniaxial deformation apparatus that provided continuous measurement of axial stress and axial strain leading to macroscopic sample failure at a constant axial strain rate of 10^{-5} s^{-1} (adhering to the International Society for Rock Mechanics suggested methods). Following the compression experiments, the remnant sample material was crushed so that a pore-free matrix density could be measured (using helium pycnometry) in order to convert the connected porosity data to total sample porosities. Henceforth the term porosity refers to the total porosity measured using a helium as the pore fluid. All samples were dried in a vacuum oven at 40 °C for at least 48 h prior to experimentation at ambient temperature and humidity. A lubricating wax was applied to both ends of the samples to limit any stress due to friction between the rock and the pistons during deformation.

In order to know the firing timescale required to ensure that thermal equilibrium was achieved in our samples we use the heat diffusion timescale λ as a scaling approximation. Given that $\lambda \approx R^2/D$ where R is the cylindrical sample radius – 10 mm – and D is the thermal diffusivity, we estimate that the time-to-equilibrium for our cylindrical samples is ~20 min. This is in agreement with fully numerical 2D simulations of heat transfer in our cylinders which are presented in the Supplementary Information along with the constraint of D as a function of porosity and the thermal properties of the pore and solid phases. We conclude that the experiments in which samples were heated for 5 h were in thermal equilibrium, whereas those heated for 10 min were not.

3. High temperature performance of vitrified wall materials

The temperature dependence of the heat capacity of Darley Dale sandstone reveals mineralogical changes and the onset of melting. We find that at heating rates of 10 and 25 °C min^{-1} the well-constrained α-to β-quartz transition (Glover et al., 1995; Heaney, 1994) occurs as a sharp endothermic spike at 577 and 579 °C, respectively, on both first and subsequent heating runs (Fig. 1a). However, the peak heat capacity associated with this transition is diminished on the second heating cycle, suggesting that quartz content has been reduced during heating to and cooling from 1400 °C (as confirmed for a compositionally similar sandstone from the Wincobank vitrified hillfort site; Wadsworth et al., 2015). A heat capacity exotherm occurs at 1002 °C for the sample heated at 10 °C min^{-1}. As heating continues, this exotherm is followed by a broad melting endotherm. The aforementioned exotherm occurs at a higher temperature of 1019 °C when heated at 25 °C min^{-1} due to the increased lag associated with heat transfer as a function of increasing heating rate. Very minor (~1%) sample mass loss occurs only on the first heating cycle with peak mass loss rates at ~650 and ~680 °C for 10 and 25 °C min^{-1}, respectively (Fig. 1b). Mass loss, associated with the dehydration of mica and clays, is therefore of negligible importance for the process of vitrification in these samples (Wadsworth et al., 2015). However, the dehydrated product of the mica and clay or the water liberated may play a crucial role in modifying the onset of melting (Friend et al., 2007).

The initial porosity of the Darley Dale sandstone is ~0.17 ± 0.005. When individual cores of the Darley Dale sandstone are thermally treated, the measured porosity increases to a maximum of ~0.25, which is a 47% increase. By contrast, when a powder aggregate of the same material is heated, the porosity decreases from ~0.45 (the initial porosity interstitial to the particles) to 0.05–0.07, which is an 84–89% decrease. During the optical dilatometry experiments,

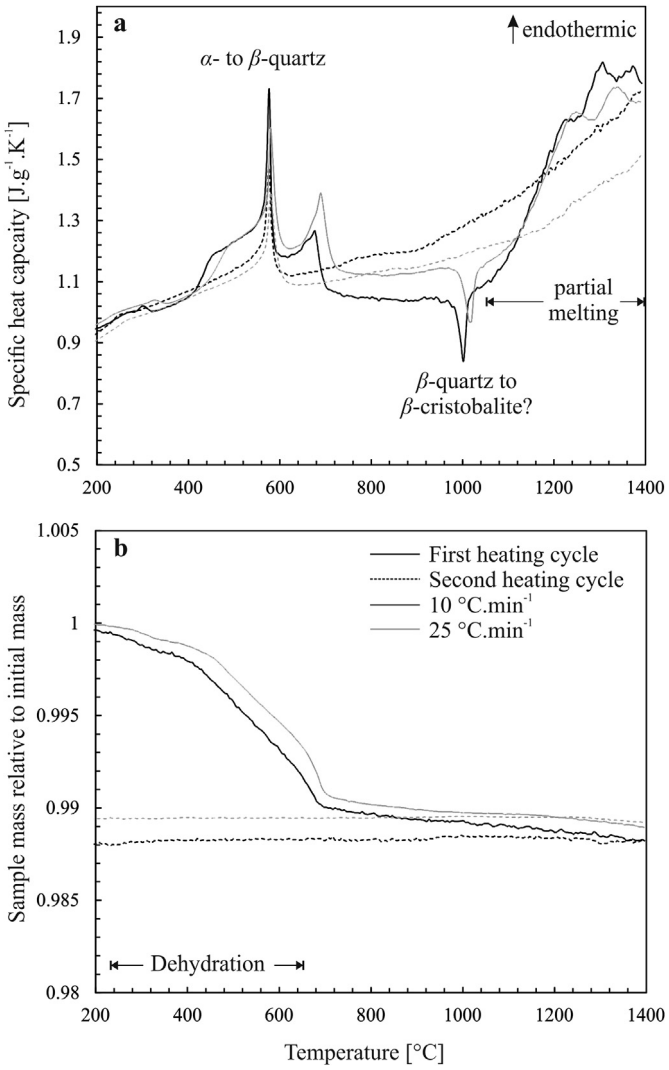

Fig. 1. The temperature dependence of specific heat capacity and sample mass determined using simultaneous thermal analysis at nominally low (10 °C min^{-1}) and high (25 °C min^{-1}) heating rates. (a) The specific heat capacity reveals the transition of α-quartz to β-quartz at 577–579 °C, the interpreted transition of β-quartz to metastable β-cristobalite at 1002–1019 °C (5), and the subsequent onset of melting at >1050 °C. (b) The temperature dependence of the sample mass normalized to the initial sample mass prior to the first heating cycle. The ~400–680 °C clay and mica dehydration process is moderately heating rate dependent.

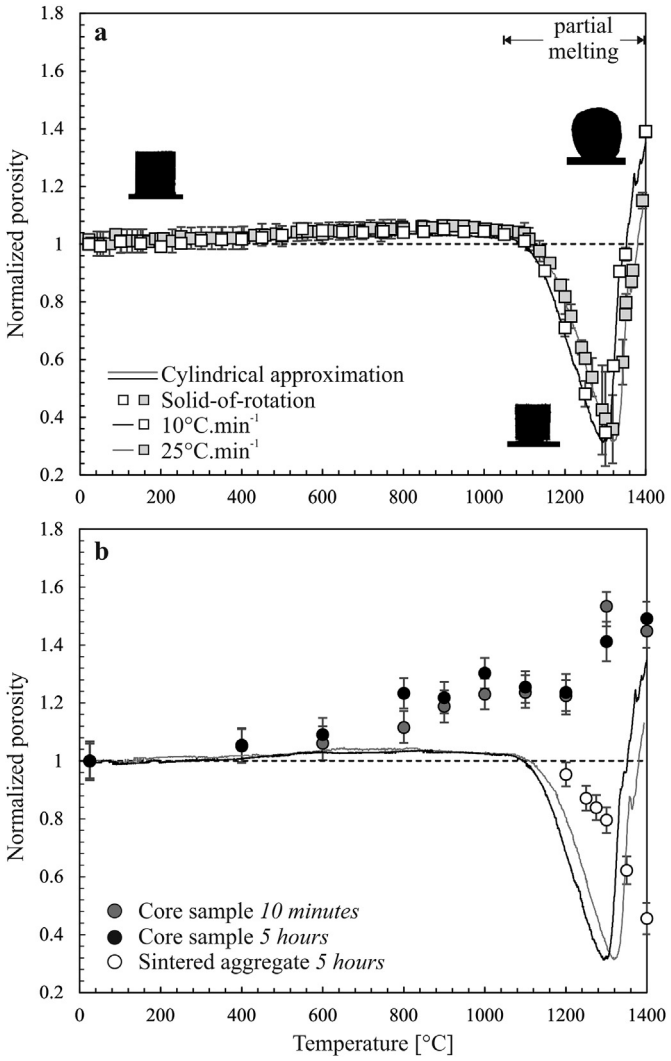

Fig. 2. The evolution of porosity normalized to the initial values in both sintered sandstones and single core sandstones. (a) The results of optical dilatometry on powder-aggregates of sandstone with examples of the binary images captured shown as examples. The cylindrical approximation of sample volume changes shows an initial thermal expansion followed by rapid sintering congruent with the onset of melting (Fig. 1) and final expansion upon pore-isolation. These data agree well with the solid-of-rotation solution. (b) Contrastingly, the core samples ubiquitously increase in porosity from the initial value at high temperature. The sintered aggregate samples decrease porosity as in (a).

after the sample reached the minimum porosity of 0.05–0.07 for both 10 and 25 °C min^{-1}, which relates to the percolation threshold of the pore-filling phase interstitial to the densifying particles, the porosity increased again to greater than the initial value of 0.45 (Fig. 2).

Heat treatment results in a dramatic increase or decrease of porosity in the heat-treated cores and powder-aggregate samples, respectively (Fig. 2). Following heat treatment, the strain response of the sample materials to an applied stress deviates from the intact material drastically depending on the conditions of treatment (as shown in the stress–strain curves of Fig. 3). The uniaxial compressive strength (the peak axial stress obtained during the experiments) of the materials is modified from that of the intact Darley Dale sandstone (Fig. 4a). The strength of the heat-treated core samples decreases as temperature increases until strength reaches a minimum at ~1100 °C. Further increase in isothermal treatment temperature results in a strength recovery, but the strength always remains below that of the intact rock. We further note that the samples held at the target temperature for 10 min are stronger than their 5 h counterparts below 1100 °C, and weaker above 1100 °C (Figs. 3 and 4). Although we find that powder-aggregate samples remain non-cohesive at temperatures ≤1100 °C, precluding sample preparation and testing, the strength non-linearly increases to values approaching that of the intact rock above this temperature (Fig. 4a). When all of the strength data are plotted as a function of porosity (as in Fig. 4b) we notice a systematic decrease in strength with increasing porosity, regardless of the experimental conditions. This commonality is further observed when the strain at failure for all of the experiments is normalized to that of the intact rock (inset in Fig. 4b). The normalized strain at failure has a peak deviation from the intact Darley Dale sandstone at the onset of melting temperature of 1100 °C, after which, for all samples, it again approaches the strain at failure for the intact rock.

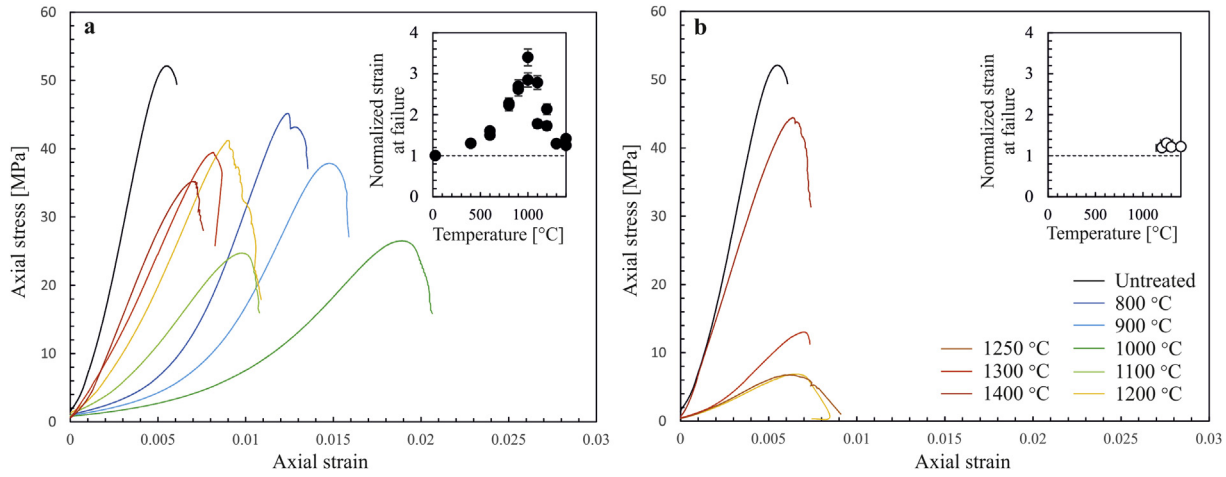

Fig. 3. Uniaxial stress–strain curves for (a) single core samples of sandstone and (b) sintered aggregate cores of sandstone prepared after exposure to different temperatures for 5 h. Insets: the strain at failure of each sample normalized by the strain at failure of the intact sandstone prior to heat treatment. The strain rate in the axial direction was 10^{-5} s^{-1} for all tests.

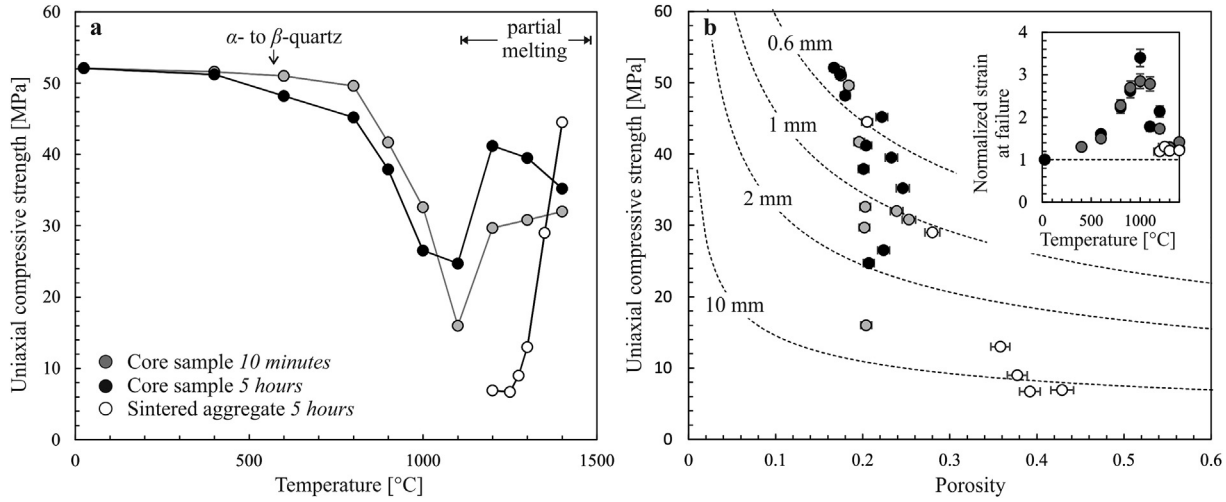

Fig. 4. The uniaxial compressive strength obtained at 10^{-5} s^{-1} deformation rate for sandstone cores and sintered samples as a function of (a) the temperature of heat treatment and (b) the resultant absolute sample porosity. In (b) the dashed lines are the result of the pore-emanating crack model for uniaxial compressive strength (see text) using a fracture toughness value for the Darley Dale sandstone of 1 MPa $m^{1/2}$ and shown for pores of equivalent radius of 10, 2, 1 and 0.6 mm. Inset: the strain at failure of each sample normalized by the strain at failure of the intact sandstone prior to heat treatment.

4. Discussion

The α-to β-quartz transition is well-established (Glover et al., 1995; Heaney, 1994) and its existence is clearly visible in our thermal treatment data (Fig. 1a). The exotherm at 1002–1019 °C for a heating rate of 10–25 °C min^{-1} (Fig. 1) is more difficult to attribute. We propose that this is related to the transition from β-quartz to a metastable β-cristobalite (Heaney, 1994; Richet et al., 1982; Wadsworth et al., 2015). This transition is non-reversible on cooling, further suggesting that β-cristobalite survives until a transition to α-cristobalite occurs at lower temperatures. As a result, α-cristobalite remains preserved in the sample at room temperature. Wadsworth et al. (2015) – studying a similar composition sandstone – noted that a non-linear decrease in the fraction of quartz was accompanied by a non-linear increase in α-cristobalite preserved at room temperature following high temperature treatment to temperatures in excess of this exotherm. The dependence of the melting endotherm on this exotherm leads us to conclude that a transition from β-quartz to β-cristobalite can induce melting of the remnant cristobalite-quartz-feldspar assemblage upon further heating by modifying the bulk solidus. While this proposal requires a thorough future thermodynamic investigation, we nevertheless find that a melt-phase is produced at temperatures in excess of the ~1002–1019 °C exotherm, which will inform our interpretation of the strength evolution of our samples discussed below.

For the solid core samples (analogues for the large blocks in the fort walls) that are subjected to high temperatures, the increase in porosity is likely initially associated with (a) thermal stress-derived microcracking or (b) microcracking associated with the α-to β-quartz phase transition, which is accompanied by a volume increase in the quartz lattice (Glover et al., 1995; Heaney, 1994). As temperature is increased from 800 to 1000 °C, the number density of thermal microcracks increases (as evidenced by the increase in porosity) and consequently strength decreases (Fig. 4a). However, above the heat-capacity exotherm (1002 at 10 °C min^{-1}; 1019 °C at 25 °C min^{-1}) we see the endothermic onset of melting (Fig. 1), which is macroscopically expressed in the samples as a colour-mottling and is manifest as the observed strength recovery

(Fig. 4a). Again we note that this strength increase does not exceed the initial strength of the intact rock. We propose that this can be explained by the partial melt fraction healing thermally-induced microcracks: a hypothesis supported by the observed reduction in curvature of the initial portion of the stress–strain curves, usually attributed to the closure of microcracks (Fig. 3). Since microcracks are known to reduce material strength (Kranz, 1983), their healing results in a pronounced strengthening (Figs. 3 & 4). In contrast, the powder-aggregate core samples (analogues for the fort wall mortar) show a consistent decrease in porosity from the initial value ~0.45. This porosity reduction is also coincident with the onset of melting observed in the heat-capacity data (Figs. 1 and 2), prior to which only minor increases in porosity are observed, attributable to minor thermal expansion. The notable porosity decrease is likely the result of sintering of the partially molten aggregate by both diffusive mass transport in the solid phases and the more rapid viscous mass transport in the melt phase (Kang, 2004; Wadsworth et al., 2014). Importantly, the porosity decrease is manifest as a bulk strength increase in the powder-aggregate core samples (Fig. 4). Optical dilatometry of powder-aggregate samples shows that the porosity increases as higher temperatures are approached because, upon isolation of a remnant porosity, the permeability of the sample falls to zero and the sample can expand due to thermal expansion of isolated pores during continually increasing temperature. Observations from vitrified forts often report molten and foamed materials (Friend et al., 2007; Youngblood et al., 1978) which could be attributable to heating of wholly sintered powders in which the isolated porosity expands. Sintering of this sort, whether diffusive or viscous, is dependent on the size of the sintering particles and the temperature dependence of the elemental mobility (diffusivity or viscosity; Kang, 2004). We note then that for all characteristic sintering timescales, large particles will sinter more slowly than small particles (Wadsworth et al., 2014). This in turn has the effect that, even if thermal equilibrium were attained in an Iron Age fort wall, the small particles interstitial to the large blocks would readily sinter, leaving the large particles less sintered. We propose that this could have a mortar effect on the bulk wall, which in engineering has long been shown to generally increase the strength of aggregate walls (Fishburn, 1961).

Sintering results in an increase in bulk material strength by (a) a reduction in porosity, (b) a reduction in pore-size and pore-size distribution (Vasseur et al., 2013) and (c) healing of microcracks. If we interrogate the pore-emanated crack model – a micromechanical model for the uniaxial compressive strength of porous materials by Sammis and Ashby (1986) – and the analytical approximation thereof (Zhu et al., 2011) we see that to a first-order, the strength of porous materials in uniaxial compression σ_u is thought to be dependent on the pore radius a, the fracture toughness K_{Ic} and the porosity ϕ. This is stated as $\sigma_u \approx \alpha K_{Ic}/(\phi^{\beta}\sqrt{\pi a})$ where α and β are the dimensionless coefficients determined by Zhu et al. (2011) as 1.325 and 0.414, respectively. This model has been shown to be effective in predicting σ_u for a variety of sandstones that have not been exposed to heat nor which have been sintered (Baud et al., 2014). A fracture toughness for the Darley Dale sandstone is 1 MPa $m^{1/2}$ (Brantut et al., 2014). However, the pore-emanating crack model is developed for an array of circular cavities in a homogeneous medium and while the solution describes the strength of intact Darley Dale sandstone with a reasonable pore radius of ~0.6 mm, it appears to overestimate the pore radii associated with the sintered aggregate materials or the thermally treated cores tested herein (Fig. 4b). Nevertheless, the fact that the data cross the pore-radii curves in Fig. 4b captures the fact that sintering is associated with a general decrease in pore radius with decreasing porosity (Kang, 2004; Vasseur et al., 2013). This gives us a micromechanical control for the major strength changes above the partial melting onset temperature of 1100 °C for the sintered powder-aggregate samples.

The key observation that the strength evolution of samples designed to represent blocks within the wall compared with initially particulate samples – the mortar holding the blocks in place – is drastically different on exposure to high temperatures introduces important subtleties to the strengthening argument for vitrification motives quickly dismissed by MacKie (1976). In the discussion below we further explore these nuances.

Vitrification temperatures at Iron Age forts are known to be high with estimates varying from biotite-induced melting at ~850 °C (Friend et al., 2007) to upper values of ~1100–1250 °C (Brothwell et al., 1974; Wadsworth et al., 2015; Youngblood et al., 1978). Even when the peak temperatures are as high as 1100–1250 °C, the time required to reach an equilibrium temperature by heat transfer through approximately meter-thick walls is large (Wadsworth et al., 2015) and can result in high temperature gradients close to the heat source akin to a contact or pyro-metamorphism scenario (Grapes, 2010). Lags in heat transfer time explain why large blocks are often less vitrified than the interstitial material. Both heat-transfer efficiency and sintering scale with particle size (Wadsworth et al., 2014). Therefore, we suggest that within a wall, the temperatures of the small mortaring particles interstitial to the largest blocks will be higher for a given distance from the heat source and these particles will undergo partial melting more rapidly and achieve a higher degree of overall partial melting. Therefore, the sintering efficiency is highly amplified in the interstices compared to the larger blocks. This is consistent with most observations that vitrified fort walls include “vitrified masses” of blocks in a glassy matrix (Brothwell et al., 1974; Friend et al., 2007; Smith and Vernioles, 1997). Specifically, Brothwell et al. (1974) show a first figure in which “angular rock fragments” are set “in a vesicular glass matrix” at the Dun Mac Uisnechan fort in Argyll, Scotland; Friend et al. (2007) show a “psammitic rubble set in a dark brown, vesicular, glass to aphanitic matrix”; and Smith and Vernioles (1997) show a first figure in which a “matrix cement” of black glass enclose angular blocks of white “sandstone or quartzite”. Childe and Thorneycroft (1938) even used “fused together” as part of their diagnostic description of a general vitrified fort. It is clear that sintering is a key and long-recognised part of the bulk wall vitrification process. However, the implications of the sintering of the small particles interstitial to the large blocks have been overlooked until now.

In rejecting the engineering motive for vitrification first proposed by Christison (1898), MacKie (1969) cites partial wall collapses that occurred in the experimental firing of Childe and Thorneycroft (1938). Examination of the experimental firing technique shows that Childe and Thorneycroft (1938) used a building “rubble” of basaltic particles crushed to 3.81–5.08 cm interstitial to large bricks of “fireclay”. This experiment was the first to show that partial vitrification was feasible using wood-fuel to fire a large wall, however, the composition and size of the rubble does not facilitate rapid sintering at the temperatures achieved. We propose that given the arbitrary size and composition of these building materials, little can be drawn about vitrification motives from such an experiment. Had the investigators taken Darley Dale sandstone, which crushes readily to the 80–800 μm particles from which it is made and which is similar in composition to the material from which the Wincobank vitrified fort in Sheffield, U.K. was built (Wadsworth et al., 2015), then they would have produced partial melts at a lower temperature than using basalts (Gualda et al., 2012). The resultant liquid droplets would have a lower sintering timescale for a given viscosity (Vasseur et al., 2013; Wadsworth et al., 2014), resulting in rapid sintering in the interstitial parts of the fort wall.

A detail can be observed when comparing our experimental results for samples heated for short (10 min) and long (5 h) times. As discussed, the largest blocks in fort walls are unlikely to be at thermal equilibrium, even if the firing of the wall lasted for days (Wadsworth et al., 2015). The Darley Dale sandstone cores we kept at the target temperature for only 10 min contained a thermal gradient and did not therefore reach thermal equilibrium, while those heated for 5 h were at equilibrium after ~0.5 h (see Supplementary Information). The strength of the cores heated for 5 h was higher for temperatures below the 1100 °C onset of partial melting than for cores heated for 10 min. This is explained simply by the fact that the center of the cores heated for 10 min did not equilibrate to the peak temperature and so any volume changes or cracking were only surficial in the sample, whereas for the cores that equilibrated, the thermal stressing or volume changes occurred throughout the sample. At peak temperatures >1100 °C in which partial melting occurred (Fig. 1), the samples that did have time to thermally equilibrate had a higher strength than the equivalent disequilibrium case. This is likely to be because more melt was produced throughout the thermal-equilibrium samples resulting in more efficient microcrack healing and porosity reduction (Fig. 2). This is another reason why large blocks not only are less likely to vitrify, but also their strength may not be as diminished as expected because they simply do not reach the peak temperatures. A scenario is envisaged in which the small particles interstitial to larger blocks are all near thermal equilibrium and >1100 °C and thus are sintering and strength is locally increasing, whereas the larger blocks are in thermal disequilibrium <1100 °C and their strength is not significantly changing. Bulk wall strength is therefore likely to increase while peak vitrification temperatures exceed the material solidus and partial melts are formed.

Fishburn (1961) showed that mortar strength is more critical to wall stability than the block or brick strength for a typical block size range. Therefore, it is likely that if structures are built of large blocks with finer interstitial material, the overall strength of the walls will increase with high temperature treatment. This is due to the sintering and strengthening of the interstitial mortaring material even though the strength of the main wall blocks may be slightly decreased. While this requires further exploration for a range of fort localities across Europe, this explanation forces a reappraisal of the once-dismissed engineering motive for Iron Age fort vitrification.

5. Conclusions

Strength and state characterization of the building stone and mortar of Iron Age forts under heating conditions indicate that Iron Age forts were strengthened by the firing to produce “vitrified” forts. The wall strength increase occurs as a result of partial melting, sintering and a resultant decrease in the porosity. The observed strengthening of Iron Age fort walls by firing to a “vitrified” state directly challenges the assumption that the motives of firing were destructive (as is currently assumed). The nature of the silicate rock-materials from which forts are built is such that the specific response of the wall stone must be carefully and individually investigated for each lithology. We therefore propose a campaign of future work on a range of fort-building lithologies in order to map their material susceptibility to Iron Age firing.

Acknowledgments

We thank Thilo Rehren for editorial handling, one anonymous reviewer for detailed comments, Jenny Schauroth and Thierry Reuschlé for experimental assistance, Jérémie Vasseur for computational support, and David E. Damby and Rebecca L. Hearne for stimulating discussion. We acknowledge support of a Procope – Hubert Curien – Partnership (PHC) grant (number 332065SG) and the ERC advanced grant “EVOKES” (explosive volcanism in the earth system: experimental insights, project number 247076).

Appendix A. Supplementary information

Supplementary information related to this article can be found at http://dx.doi.org/10.1016/j.jas.2016.01.011.

References

Aylwin Cotton, M., 1954. British camps with timber-laced ramparts. Archaeol. J. 111 (1), 26–105.
Baud, P., Wong, T.-F., Zhu, W., 2014. Effects of porosity and crack density on the compressive strength of rocks. Int. J. Rock Mech. Min. Sci. 67, 202–211.
Bowden, M., McOmish, D., 1987. The required barrier. Scott. Archaeol. Rev. 4 (2), 76–84.
Brantut, N., Heap, M., Baud, P., Meredith, P., 2014. Rate-and strain-dependent brittle deformation of rocks. J. Geophys. Res. Solid Earth 119 (3), 1818–1836.
Brothwell, D., Bishop, A., Woolley, A., 1974. Vitrified forts in Scotland: a problem in interpretation and primitive technology. J. Archaeol. Sci. 1 (1), 101–107.
Childe, V.G., Thorneycroft, W., 1938. The experimental production of the phenomena distinctive of vitrified forts. Proc. Soc. Antiq. Scotl. 12 (1937), 44–55.
Christison, D., 1898. Early Fortifications in Scotland: Motes, Camps, and Forts. W. Blackwood and Sons. Blackwood, Edinburgh.
Fishburn, C.C., 1961. Effect of Mortar Properties on Strength of Masonry.
Friend, C., Dye, J., Fowler, M., 2007. New field and geochemical evidence from vitrified forts in South Morar and Moidart, NW Scotland: further insight into melting and the process of vitrification. J. Archaeol. Sci. 34 (10), 1685–1701.
Gifford, J., 1992. Highland and Islands. Yale University Press.
Glover, P., Baud, P., Darot, M., Meredith, P., Boon, S., LeRavalec, M., Zoussi, S., Reuschle, T., 1995. α/β phase transition in quartz monitored using acoustic emissions. Geophys. J. Int. 120 (3), 775–782.
Grapes, R., 2010. Pyrometamorphism. Springer Science & Business Media, p. 277.
Gualda, G.A., Ghiorso, M.S., Lemons, R.V., Carley, T.L., 2012. Rhyolite-MELTS: a modified calibration of MELTS optimized for silica-rich, fluid-bearing magmatic systems. J. Petrol. 53 (5), 875–890.
Hajpál, M., 2002. Changes in sandstones of historical monuments exposed to fire or high temperature. Fire Technol. 38 (4), 373–382.
Heaney, P.J., 1994. Structure and chemistry of the low-pressure silica polymorphs. Rev. Mineral. Geochem. 29 (1), 1–40.
Heap, M., Baud, P., Meredith, P., Bell, A., Main, I., 2009. Time-dependent brittle creep in Darley Dale sandstone. J. Geophys. Res. Solid Earth 1978–2012 114 (B7).
Heap, M.J., Lavallee, Y., Laumann, A., Hess, K.U., Meredith, P.G., Dingwell, D.B., 2012. How tough is tuff in the event of fire? Geology 40 (4), 311–314.
Kang, S.-J.L., 2004. Sintering: Densification, Grain Growth and Microstructure. Butterworth-Heinemann.
Kranz, R.L., 1983. Microcracks in rocks: a review. Tectonophysics 100 (1), 449–480.
Kresten, P., Goedicke, C., 1996. TL-dating of vitrified forts: did Birnam Wood go to Dunsinane Hill in AD455. Iskos 11, 99–106.
MacKie, E., 1969. Timber-laced and vitrified walls in Iron Age forts: causes of vitrification. Glasg. Archaeol. J. 69–71.
MacKie, E.W., 1976. The Vitrified Forts of Scotland: Hillforts, Later Prehistoric Earthworks in Britain and Ireland. Academic Press, London, pp. 205–235.
Nisbet, H.C., 1974. A geological approach to vitrified forts. Sci. Archaeol. 12, 3–12.
Ralston, I., 1986. The Yorkshire Television vitrified wall experiment at East Tullos, City of Aberdeen District. In: Proceedings of the Society of Antiquaries of Scotland, 116. National Museum of Antiquities of Scotland, pp. 17–40.
Ralston, I., 2007. Celtic fortifications in the British Isles. In: Proceedings Celtic fortifications in the British Isles, 20. Real Academia de la Historia et Casa de Velázquez., Madrid, pp. 113–134.
Richet, P., Bottinga, Y., Denielou, L., Petitet, J., Tequi, C., 1982. Thermodynamic properties of quartz, cristobalite and amorphous SiO 2: drop calorimetry measurements between 1000 and 1800 K and a review from 0 to 2000 K. Geochim. Cosmochim. Acta 46 (12), 2639–2658.
Sammis, C., Ashby, M., 1986. The failure of brittle porous solids under compressive stress states. Acta Metall. 34 (3), 511–526.
Small, A., Cottam, M., 1972. Craig Phaidrig. In: Occasional Papers, vol. 1. University of Dundee, Department of Geography.
Smith, D.C., Vernioles, J.D., 1997. The temperature of fusion of a celtic vitrified Fort: a feasibility study of the application of the Raman microprobe to the non-destructive characterization of unprepared archaeological objects. J. Raman Spectrosc. 28 (2–3), 195–197.
Vasseur, J., Wadsworth, F.B., Lavallée, Y., Hess, K.U., Dingwell, D.B., 2013. Volcanic sintering: timescales of viscous densification and strength recovery. Geophys. Res. Lett. 40 (21), 5658–5664.
Wadsworth, F.B., Vasseur, J., Aulock, F.W., Hess, K.U., Scheu, B., Lavallée, Y., Dingwell, D.B., 2014. Nonisothermal viscous sintering of volcanic ash. J. Geophys. Res. Solid Earth 119, 8792–8804.
Wadsworth, F.B., Damby, D.E., Hearne, R.L., Le Blond, J.S., Vasseur, J., Najorka, J., Hess, K.-U., Dingwell, D.B., 2015. The feasibility of vitrifying a sandstone

enclosure in the British Iron Age. J. Archaeol. Sci. Rep. 4, 605–612.
Wu, X.Y., Baud, P., Wong, T.-F., 2000. Micromechanics of compressive failure and spatial evolution of anisotropic damage in Darley Dale sandstone. Int. J. Rock Mech. Min. Sci. 37 (1), 143–160.
Youngblood, E., Fredriksson, B., Kraut, F., Fredriksson, K., 1978. Celtic vitrified forts: implications of a chemical-petrological study of glasses and source rocks. J. Archaeol. Sci. 5 (2), 99–121.
Zhu, W., Baud, P., Vinciguerra, S., Wong, T. f, 2011. Micromechanics of brittle faulting and cataclastic flow in Alban Hills tuff. J. Geophys. Res. Solid Earth 1978–2012 116 (B6).